

539-34
2002-04

LONG-WAVELENGTH INSTABILITY IN MARANGONI CONVECTION

Stephen J. Van Hook, Michael F. Schatz, Jack B. Swift,
W. D. McCormick and Harry L. Swinney
Center for Nonlinear Dynamics and Department of Physics
The University of Texas at Austin
Austin, TX 78712

LT

ABSTRACT

Our experiments in thin liquid layers (~ 0.1 mm thick) heated from below reveal a well-defined long-wavelength instability: at a critical temperature difference across the layer, the depth of the layer in the center of the cell spontaneously decreases until the liquid-air interface ruptures and a dry spot forms. The onset of this critical instability occurs at a temperature difference across the liquid layer that is 35% smaller than that predicted in earlier theoretical studies of a single layer model. Our analysis of a two-layer model yields predictions in accord with the observations for liquid layer depths ≥ 0.15 mm, but for smaller depths there is an increasing difference between our predictions and observations (the difference is 25% for a layer 0.06 mm thick). In microgravity environments the long-wavelength instability observed in our terrestrial experiments is expected to replace cellular convection as the primary instability in thick as well as thin liquid layers heated quasistatically from below.

INTRODUCTION

An understanding of thermocapillary flows and other surface-tension-driven phenomena will be critical for successful containerless processing in microgravity. Surface-tension-driven Bénard (Marangoni) convection (see Fig. 1), in which a liquid with a free upper surface is heated from below, is a classic example of such thermocapillary flows. The temperature gradient on the free surface that initially drives the fluid flow can originate from both temperature fluctuations and deformational perturbations. The former are stabilized by diffusion, the latter by gravity. When gravity is sufficiently strong to stabilize deformational perturbations, the primary instability leads to the short-wavelength hexagonal convection cells first observed by Bénard [1]. This instability forms when the Marangoni number ($M \equiv \sigma_T \Delta T d / \rho \nu \kappa$), the non-dimensionalized ΔT across the liquid, exceeds a critical value M_c . Recent experiments have yielded $M_c = 83$ [2], in accord with linear stability theory [3]. In microgravity, however, another instability can arise; the liquid is particularly vulnerable to deformational instabilities since gravity (characterized by the Galileo number, $G \equiv g d^3 / \nu \kappa$, where g is the gravitational acceleration) is not strong enough to prevent thermocapillarity (characterized by M) from pulling liquid from warm, depressed regions of the interface to cool, elevated regions. The suppression of curvature by surface tension causes this deformational instability to appear with a long wavelength.

This long-wavelength instability was predicted to exist in the 1960's [4, 5], but the present experiments are the first to demonstrate the existence of this instability [6]. Both linear [7-9] and nonlinear [10-13] theories have used a one-layer model, with the effect of the air layer modeled by use of a heat transfer coefficient, the Biot number, which in the long-wavelength limit is $H = k_a d / k d_a$, where k and k_a , respectively, are the liquid and air thermal conductivities and d and d_a are the layer thicknesses. The one-layer model predicts onset of the instability at $M = (2/3)G(1 + H)$. To study this long-wavelength instability in terrestrial experiments, we achieve small G by using very thin depths, $d \sim 0.1$ mm; a 0.1-mm-thick layer of liquid in terrestrial gravity has the same G as a 1.0-mm-thick layer for $g = 10^{-3}g_E$.

EXPERIMENTAL METHODS

We study a thin layer of silicone oil that lies on a heated, gold-plated aluminum mirror and is bounded above by an air layer (see Fig. 1). A single-crystal sapphire window (0.3-cm-thick) above the air is cooled by a temperature-controlled chloroform bath. The temperature drop across the liquid layer is calculated assuming conductive heat transport and is typically 0.5–5 °C. We use a distilled polydimethylsiloxane silicone oil with a viscosity of 10.2 cS at 50 °C [14]. The circular cell (3.81 cm inner diameter) has aluminum sidewalls whose upper surface is made non-wetting with a coating of Scotchgard. The liquid layers are sufficiently thin that buoyancy is negligible; the experiments are performed with $0.005 \text{ cm} < d < 0.025 \text{ cm}$ (with aspect ratios ranging from 150 to 750) and $0.023 < d_g < 0.080 \text{ cm}$ (typically $d_g = 0.035 \text{ cm}$); the corresponding fundamental wavevectors are in the range $0.008 < q = 2\pi d/L < 0.040$ ($\ll 1$). We visualize the layer using interferometry, shadowgraph and infrared imaging (256×256 pixel InSb staring array, sensitive in the range 3–5 μm). The gap between the sapphire window and the mirror is uniform to 1%, as verified interferometrically. The liquid surface is initially flat and parallel to the mirror to 1% in the central 90% of the cell, with a boundary region near the sidewalls due to contact line pinning. This initial depth variation is accentuated by thermocapillarity as ΔT is increased; measurements of depth variation show a 10% surface deformation in the central 90% of the cell at 3% below onset.

EXPERIMENTAL RESULTS

Instability Onset Above a critical ΔT , the liquid layer becomes unstable to a long-wavelength draining mode that eventually forms a dry spot [see Figs. 2(left) and 5(left)]. The drained region takes several hours (of order a horizontal diffusion time, L^2/κ) to form. Although we refer to the drained region as a “dry spot”, it is not completely dry since an adsorbed layer $\sim 1 \mu\text{m}$ thick remains. The size of the drained region is typically one-quarter to one-third the diameter of the entire cell. As Fig. 3(left) shows, our measurements of onset are consistently 35% below in ΔT (or M) the prediction of linear stability for the one-layer model that appears in the literature [7–13]. We do not believe this discrepancy is due to systematic errors in the characterization of our experiment (*e.g.*, geometry, fluid properties) or nonuniform heating of the liquid because experiments in the same convection cell using thicker liquid layers find onset of hexagons uniform across the cell at a ΔT that agrees with another experiment [2] and linear stability theory [3].

Mode Competition The long-wavelength and the hexagonal modes become simultaneously unstable at a critical liquid depth d_c . Near this critical depth, both modes of instability compete and influence the formation of the pattern. The two modes are not mutually exclusive, but there is a fundamental imbalance in their relationship: the presence of the hexagons suppresses the long-wavelength mode, while the presence of long-wavelength deformation may induce the formation of hexagons. One-layer linear stability theory predicts $d_c = (120\nu\kappa/g)^{1/3} = 0.023 \pm 0.001 \text{ cm}$; we observe the exchange of primary instabilities at $d_c = 0.025 \pm 0.001 \text{ cm}$. For $d > d_c$, hexagons are the primary instability [see Fig. 2(right)]; the hexagons smooth the large-scale temperature variations that would allow formation of the long-wavelength mode as a secondary instability when M exceeds M_c .

For $d < d_c$, the long-wavelength mode is the primary instability. The liquid expelled from the forming dry spot increases the local height $h(x, y, t)$ and thus the local Marangoni number [$\propto h(x, y, t)$] in the newly formed elevated region; for $0.017 \text{ cm} < d < d_c$, hexagons form in the elevated region since the local M in this region exceeds M_c for the onset of hexagons [see Fig. 2(center)]. For $d < 0.017 \text{ cm}$, hexagons do not form at the onset of the long-wavelength mode [see Fig. 2(left)], but can form in the elevated region for ΔT sufficiently far above onset. Similar mode

competition phenomena have been studied theoretically for solutocapillary convection [15]. Rapid instead of quasistatic ramping can lead to the formation of the hexagons where the long-wavelength is predicted to be the primary instability since the timescale for formation of hexagons (the vertical diffusion time, d^2/κ) is much shorter than the timescale for formation of the long-wavelength mode (the horizontal diffusion time, L^2/κ). When $d \ll d_c$, increasing ΔT far above ΔT_c increases the area of the dry spot until the remaining layer is thick enough to form hexagons, which then halts any further advance of the dry spot. At fixed ΔT , the dry spot is stable.

TWO-LAYER MODEL

The evolution of the instability can be studied using a nonlinear evolution equation derived from the Navier-Stokes equations in the limit of long-wavelengths. Several authors [10-13] have derived evolution equations using a one-layer model. We have developed a two-layer model which takes into account the change in the temperature profile in the air due to deformation of the interface. The appropriate heat transfer coefficient then becomes $F = (d/d_a - H)/(1 + H)$. The two-layer model reduces to the one-layer model in the limit $d/d_a \rightarrow 0$. The two-layer evolution equation for the surface height $h(x, y, t)$ is:

$$\frac{3}{G} h_t + \nabla \cdot \left\{ \frac{3M}{2G} \frac{(1+F) h^2 \nabla h}{(1+F-Fh)^2} - h^3 \nabla h + \left(\frac{2\pi d}{L} \right)^2 \frac{h^3}{B_L} \nabla^2 \nabla h \right\} = 0$$

where time is scaled by d^2/κ and B_L is a modified static Bond number, $B_L \equiv \rho g(L/2\pi)^2/\sigma > 0$. $B_L \sim 30$ for our experiments. The first term in curly brackets describes the effect of thermocapillarity; the second, gravity; and the third, surface tension.

Analysis A linear stability analysis of the above equation predicts onset of the instability at

$$M = \frac{2G}{3(1+F)},$$

which is smaller than predicted by the one-layer model. As d/d_a increases, the difference between the two theories becomes more pronounced. A weakly nonlinear analysis of the evolution equation reveals that the bifurcation is subcritical for all B_L and F , with squares being more unstable than rolls. We solved for all the steady states in one dimension (rolls) and discovered that no stable, deformed states exist; that is, the bifurcation curve continues backwards in M , never turning over in a saddle-node bifurcation. The shape of the (unstable) steady states changes at $F = 1/2$, and thus the two-layer model suggests a qualitative change in behavior at $F = 1/2$. The two-layer model reduces to the one-layer model when $d/d_a = 0$ and thus $F \leq 0$, so the one-layer model cannot make this prediction.

Numerical Simulations We performed numerical simulations of the evolution equation, both with a one-dimensional and a two-dimensional surface. The simulations employed a pseudospectral method to handle the extreme nonlinearity of the equations. Because of the fourth-order nonlinearity, a 2/5 rule was required to prevent aliasing (e.g., for 256 spatial locations in one dimension, only 103 spectral modes from -51 to +51 were used). At each time-step, the power in the remaining 3/5 of modes was exponentially damped. We used periodic boundary conditions (a square box in two-dimensions) with a Fourier series as a basis set. The simulations find the same bifurcation curve as the analytical theory found. When the system is unstable, it forms either a dry spot ($F < 1/2$) or an elevated region ($F > 1/2$), as Fig. 4 illustrates. The evolution equation gives good qualitative agreement to the experiments for $F < 1/2$ (see Fig. 5).

CONCLUDING REMARKS

Terrestrial experiments produce the first observation of a long-wavelength deformational instability in surface-tension-driven Marangoni convection. The experimental results do not agree with a one-layer model in the literature, but do agree with a two-layer model for certain liquid depths. The source of the deviation from the two-layer model is being investigated.

The two-layer model predicts a qualitatively different state, one with an elevated region, for sufficiently large d/d_a ($F > 1/2$); we are currently testing this prediction. Employing gases other than air (*e.g.*, helium) allows us to vary F without changing the geometry of the experiment or the liquid layer thickness.

ACKNOWLEDGMENTS

We thank S.H. Davis and R.E. Kelly for helpful discussions. This research is supported by the NASA Microgravity Science and Applications Division (Grant No. NAG3-1382). S.J.V.H. is supported by the NASA Graduate Student Researchers Program.

REFERENCES

- [1] H. Bénard, *Rev. Gén. Sci. Pure Appl.* **11**, 1261 (1900).
- [2] M. F. Schatz, S. J. VanHook, W. D. McCormick, J. B. Swift and H. L. Swinney, *Phys. Rev. Lett.* **75**, 1938 (1995).
- [3] J. R. A. Pearson, *J. Fluid Mech.* **4**, 489 (1958).
- [4] L. E. Scriven and C. V. Sternling, *J. Fluid Mech.* **19**, 321 (1964).
- [5] K. A. Smith, *J. Fluid Mech.* **24**, 401 (1966).
- [6] S. J. Van Hook, M. F. Schatz, W. D. McCormick, J. B. Swift, and H. L. Swinney, *Phys. Rev. Lett.* **75**, 4397 (1995).
- [7] M. Takashima, *J. Phys. Soc. Japan* **50**, 2745 (1981).
- [8] D. A. Goussis and R. E. Kelly, *Int. J. Heat Mass Trans.* **33**, 2237 (1990).
- [9] C. Pérez-García and G. Carneiro, *Phys. Fluids A* **3**, 292 (1991).
- [10] S. H. Davis, in *Waves on Fluid Interfaces*, edited by R. E. Meyer (Academic Press, New York, NY, 1983), p. 291.
- [11] S. H. Davis, *Annu. Rev. Fluid Mech.* **19**, 403 (1987).
- [12] B. K. Kopbosynov and V. V. Pukhnachev, *Fluid Mech. Sov. Res.* **15**, 95 (1986).
- [13] A. Oron and P. Rosenau, *J. Phys. II (France)* **2**, 131 (1992).
- [14] M. F. Schatz & K. Howden, *Exp. in Fluids* **19**, 359 (1995).
- [15] A. A. Golovin, A. A. Nepomnyashchy and L. M. Pismen, *Phys. Fluids* **6**, 34 (1994).

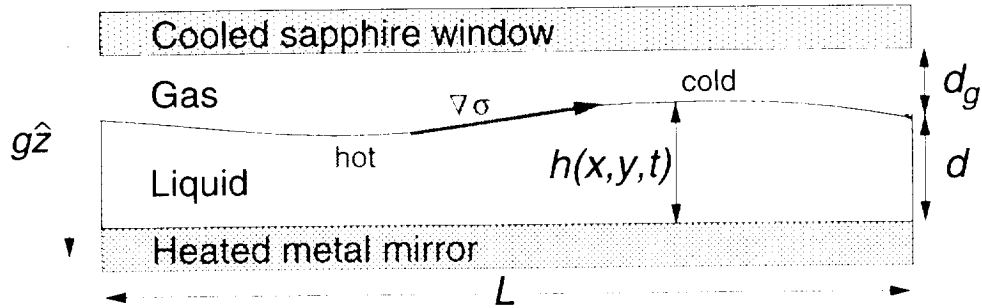


Fig. 1. Sketch of Marangoni convection experiment. Silicone oil (depth d) is heated from below and is bounded above by an air layer (depth d_a). The air layer is cooled from above and the mean temperature drop across the liquid layer is ΔT . In the presence of deformation, a temperature-gradient-induced surface-tension gradient pulls liquid against gravity up the interface. The liquid has density ρ , kinematic viscosity ν , thermal conductivity k , thermal diffusivity κ , and temperature coefficient of surface tension $\sigma_T \equiv |d\sigma/dT|$.

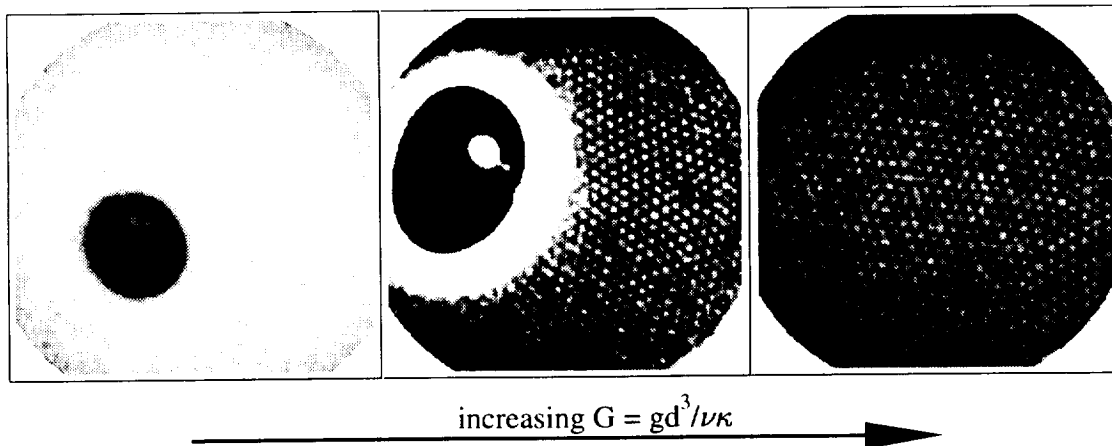


Fig. 2. Infrared images from experiments with increasing liquid depth (increasing G). Left: For $d = 0.011$ cm, the long-wavelength mode is the primary instability. The dark region is the dry spot. Center: At $d = 0.022$ cm, the long-wavelength and hexagonal modes coexist. A droplet (white circle) is trapped within the dry spot (dark oval); the liquid layer is strongly deformed (white annulus) between the dry spot and the hexagonal pattern. Right: For $d > 0.025$ cm (in air), hexagons are the primary instability (here $d = 0.033$ cm).

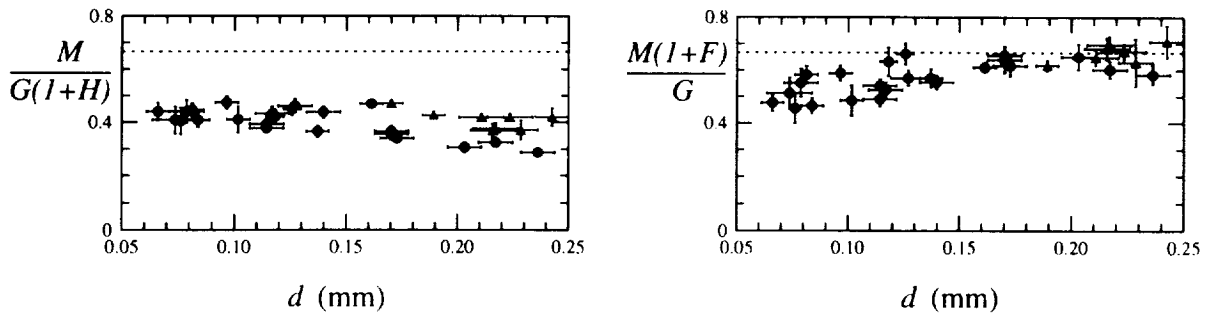


Fig. 3. Comparison of the observed instability onset to both (left) one- and (right) two-layer linear stability theory (dashed line). Circles correspond to dry spots, triangles to dry spots with hexagons. For $d > 0.18$ mm, the circles are from experiments in which He, not air, was used as the gas. The data agree well with the two-layer theory for thick liquid depths, but not for thin liquid depths.

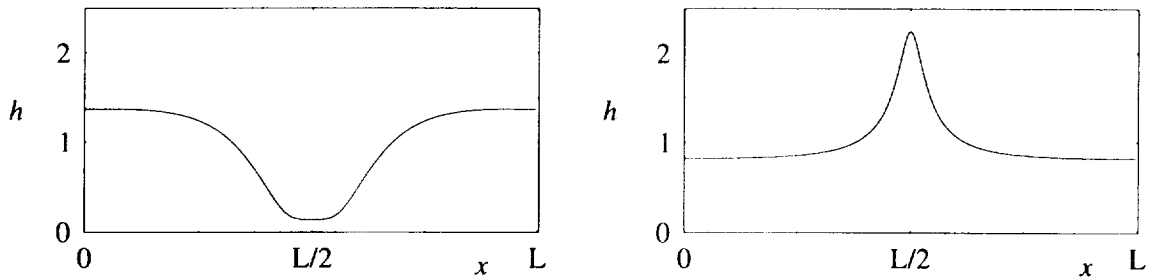


Fig. 4. The height of the layer as a function of position in the cell as determined by one-dimensional numerical simulations for two values of F at 0.33% above the onset of linear instability. Left: $F = 1/3$, $B_L = 30$. A dry spot forms where the depth of the liquid nearly approaches zero in the drained region. Right: $F = 2/3$, $B_L = 30$. The system forms a localized elevated region instead of a dry spot. It continues to evolve until it ‘hits’ the top plate.

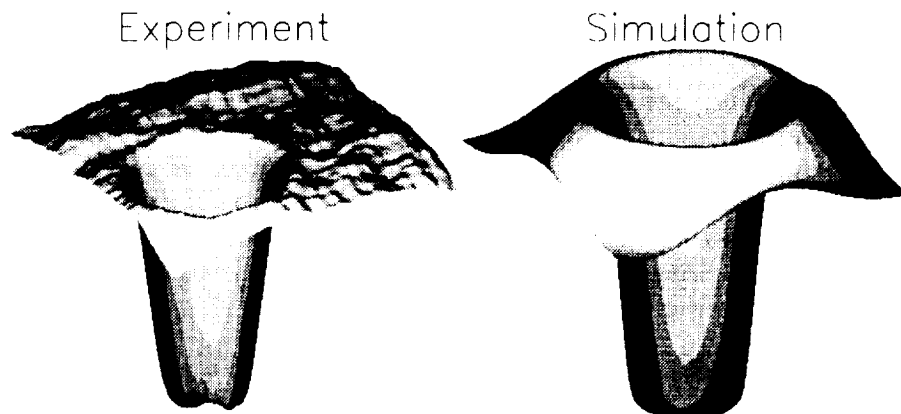


Fig. 5. Dry spot in both experiment and numerical simulation. The experimental picture shows the measured brightness temperature as a function of position along the interface about 10% above onset of instability; $d = 0.011$ cm ($F \sim 0.2$). Numerical simulation of a long-wavelength evolution equation ($F = 0$, $B_L = 30$) shows the depth as a function of position for 1% above onset of linear instability. The depth of the liquid approaches zero in the drained region.